Journal of Applied Polymer Science

Removal of Cr(VI) from aqueous solution using amino-modified Fe_3O_4-SiO_2-chitosan magnetic microspheres with high acid resistance and adsorption capacity

Xitong Sun,[1,2,3] Liangrong Yang,[2] Tingting Dong,[2,3] Zhini Liu,[2,4] Huizhou Liu[1,2]

[1]CAS Key Laboratory of Biobased Materials, Qingdao Institute of Bioenergy and Bioprocess Technology, Chinese Academy of Sciences, Qingdao 266101, People's Republic of China

[2]Key Laboratory of Green Process and Engineering, Institute of Process Engineering, Chinese Academy of Sciences, Beijing 100190, People's Republic of China

[3]University of Chinese Academy of Sciences, Beijing 100049, People's Republic of China

[4]College of Chemical Engineering, Xiangtan University, Xiangtan 411105, People's Republic of China

Correspondence to: L. Yang (E-mail: lryang@ipe.ac.cn) and H. Liu (E-mail: hzliu@ipe.ac.cn)

ABSTRACT: A novel, bioadsorbent material of polyethylenimine-modified magnetic chitosan microspheres enwrapping magnetic silica nanoparticles (Fe_3O_4–SiO_2–CTS-PEI) was prepared under relatively mild conditions. The characterization results indicated that the adsorbent exhibited high acid resistance and magnetic responsiveness. The Fe_3O_4 loss of the adsorbent was measured as 0.09% after immersion in pH 2.0 water for 24 h, and the saturated magnetization was 11.7 emu/g. The introduction of PEI obviously improved the adsorption capacity of Cr(VI) onto the adsorbent by approximately 2.5 times. The adsorption isotherms and kinetics preferably fit the Langmuir model and the pseudo-second-order model. The maximum adsorption capacity was determined as 236.4 mg/g at 25°C, which was much improved compared to other magnetic chitosan materials, and the equilibrium was reached within 60 to 120 min. The obtained thermodynamic parameters revealed the spontaneous and endothermic nature of the adsorption process. Furthermore, the Cr(VI)-adsorbed adsorbent could be effectively regenerated using a 0.1 mol/L NaOH solution, and the adsorbent showed a good reusability. Due to the properties of good acid resistance, strong magnetic responsiveness, high adsorption capacity, and relatively rapid adsorption rate, the Fe_3O_4–SiO_2–CTS-PEI microspheres have a potential use in Cr(VI) removal from acidic wastewater.
 J. Appl. Polym. Sci. **2016**, *133*, 43078.

KEYWORDS: applications; adsorption; biomaterials; emulsion polymerization; magnetism and magnetic properties

Received 15 March 2015; accepted 22 October 2015

DOI: 10.1002/app.43078

INTRODUCTION

In recent years, the damage to water resources from the rapid development of industrial technologies has become an important factor impacting economic and social development. Chromium and its compounds are important industrial chemicals that are extensively used in leather tanning, electroplating, textile dying, pigment manufacture, and metal polishing.[1,2] However, the Cr(VI)-containing effluents from these industries pose a serious threat to the environment and human health because of their carcinogenic and mutagenic properties.[3–5] To solve this problem, several technologies have been applied for Cr(VI) removal, such as chemical reduction and precipitation, electrodialysis, membrane filtration, ion exchange, and adsorption.[6–9] The majority of these methods suffer from high technological equipment and operation costs, but adsorption is considered as an economic and cost-effective method.

Currently, bioadsorbents based on microorganism cells,[10] cellulose,[11] chitosan,[12,13] and agricultural wastes[14] were developed and widely used for Cr(VI) removal, with the advantages of low cost, nontoxicity, and abundant sources. Among these biomaterials, chitosan (CTS) should be considered as an effective candidate for Cr(VI) removal owing to the characteristics of low cost, hydrophilicity, biodegradability, biocompatibility, and plenty of functional groups (—NH_2 and —OH) on the macromolecular chain.[12,13] However, the traditional chitosan-based adsorbents cannot be separated from the wastewater easily

Additional Supporting Information may be found in the online version of this article.

except by high-speed centrifugation or filtration. At present, several kinds of magnetic chitosan-based adsorbents have been developed for the treatment of Cr(VI)-containing wastewater,[15–19] and they can be easily and quickly recovered from wastewater only by applying an external magnetic field. Unfortunately, most of these magnetic chitosan-based adsorbents in the previous works had a low adsorption capacity, which limited their practical application. The chitosan-coated $MnFe_2O_4$ nanoparticles were prepared and tested for their ability to remove Cr(VI), and the maximum adsorption capacity was only 35.323 mg/g.[16] Hu *et al.* studied the removal of Cr(VI) using a ethylenediamine-modified crosslinked magnetic chitosan resin, with a maximum adsorption capacity of 51.813 mg/g.[18] Therefore, exploration of a magnetic chitosan adsorbent with high adsorption capacity has great realistic meaning.

Furthermore, the adsorption of Cr(VI) in the previous studies was usually performed under acidic conditions in the pH range of 2.0–6.0.[20–22] However, the most widely used magnetic core of magnetic adsorbents was iron oxide, and it tended to leach out in an acidic environment. Thus a protective coating was necessary on the surface of the iron oxide. SiO_2 is very stable in an acidic environment and can be recognized as an ideal shell composite to protect the inner magnetic core.[23–25] In the previous work, the EDTA-modified chitosan composite enwrapping magnetic silica microspheres was prepared and employed for the removal of Cu(II), Pb(II), and Cd(II) ions,[26] but the morphology of the material was irregular, and some magnetic silica microspheres were not embedded inside the crosslinked chitosan. The emulsion crosslinking method[27] would be a good choice to solve this problem, in which the magnetic silica nanoparticles were used as the magnetic cores. To the best of our knowledge, the preparation of Fe_3O_4–SiO_2–CTS microspheres using the emulsion crosslinking technique has not been reported.

Amino groups demonstrate an outstanding ability in the removal of Cr(VI),[28–31] and branch polyethylenimine (PEI) can be recognized as an effective reagent to modify the adsorbent owing to the large number of amino groups on the molecular chain. In this study, in order to improve the acid resistance and adsorption capacity of the adsorbent, the PEI-modified magnetic chitosan microspheres enwrapping magnetic silica nanoparticles were prepared and well characterized. Next, the resulting microspheres were used as a novel adsorbent to remove Cr(VI) from an acidic aqueous solution, with the advantages of strong magnetic responsiveness, good acid resistance, and high adsorption capacity.

EXPERIMENTAL

Materials and Chemicals

PEI (10,000, 50% solution in water) was purchased from Sigma-Aldrich (St. Louis, MO). Powdery chitosan (degree of deacetylation: 80.0∼95.0%, molecular weight: 1.3×10^5 Da), ferric chloride hexahydrate ($FeCl_3{\cdot}6H_2O$), ferrous chloride tetrahydrate ($FeCl_2{\cdot}4H_2O$), concentrated ammonium hydroxide ($NH_3{\cdot}H_2O$, 25%), sodium citrate ($C_6H_5O_7Na_3{\cdot}2H_2O$), tetraethyl orthosilicate (TEOS), acetic acid, mineral oil, petroleum ether, Tween-80, glutaraldehyde (25% solution in water), *N*,*N*-dimethylformamide (DMF), and methylacrylate (MA) were of analytical grade and obtained from Sinopharm Chemical Reagent Co. (Beijing, China).

Preparation of Fe_3O_4–SiO_2–CTS-PEI Microspheres

The synthesis route of Fe_3O_4–SiO_2–CTS-PEI microspheres is illustrated in Scheme 1. The citric acid–modified Fe_3O_4 nanoparticles were first synthesized using the coprecipitation method according to our previous work and then were coated with SiO_2 by the sol-gel method.[32,33] Next, the Fe_3O_4–SiO_2–CTS microspheres were prepared by the emulsion crosslinking method.[27] Finally, the PEI was grafted onto the surface of the microspheres using a Michael addition reaction and an amidation reaction.[34,35] The detailed experimental procedures of preparation of the adsorbent are provided in the Supporting Information.

Characterization

The morphologies of Fe_3O_4, Fe_3O_4–SiO_2, Fe_3O_4–SiO_2–CTS, and Fe_3O_4–SiO_2–CTS-PEI were characterized by transmission electron microscopy (TEM, JEM-2010, Japan) and scanning electron microscopy (SEM, JEOL JSM-6700F, Japan). Fourier transform infrared (FTIR) spectra of Fe_3O_4, Fe_3O_4–SiO_2, Fe_3O_4–SiO_2–CTS, Fe_3O_4–SiO_2–CTS-MA (reaction intermediate), and Fe_3O_4–SiO_2–CTS-PEI were recorded on a spectrophotometer (Bruker T27, Germany) between 4000 and 400 cm^{-1}. X-ray diffraction (XRD, Smartlab 9, Japan) was used to analyze the crystal structure of Fe_3O_4, chitosan, Fe_3O_4–SiO_2–CTS, and Fe_3O_4–SiO_2–CTS-PEI. The magnetic properties of Fe_3O_4–SiO_2–CTS-PEI were determined by a vibrating sample magnetometer (VSM, LakeShore 7307, USA) at room temperature. Thermogravimetric analysis (TGA, Netzsch STA 449C, Germany) of Fe_3O_4–SiO_2–CTS-PEI was carried out from room temperature to 900°C with a heating rate of 10°C/min under steady nitrogen. The specific surface area of Fe_3O_4–SiO_2–CTS-PEI was examined by an automated gas sorption analyzer (Quantachrome Autosorb-1-C-TCD, USA) according to the Brunauer-Emmett-Teller (BET) method. The average pore diameter and porosity of Fe_3O_4–SiO_2–CTS-PEI were determined by a mercury porosimeter (Monitor AutoPore IV 9510, USA). The amino group capacities of Fe_3O_4–SiO_2–CTS and Fe_3O_4–SiO_2–CTS-PEI were estimated using the volumetric method according to our previous work.[35] The Cr2p XPS spectrum was obtained with an X-ray photoelectron spectrometer (ESCALAB 250Xi, Thermo, USA).

Adsorption Experiments

The effects of pH, adsorbent dose, initial Cr(VI) concentration, contact time, temperature, coexisting ion competition, and reusability were tested in a batch method. Typically, 50 mL of a solution of known Cr(VI) concentration and 25 mg of Fe_3O_4–SiO_2–CTS-PEI microspheres were added to 100 mL glass flasks and then agitated in a water bath shaker at 150 rpm. The temperature was kept within ±1°C of the set value, and the pH value of the solution was adjusted by a 1 mol/L HCl solution or a 1 mol/L NaOH solution. The effect of the common coexisting ions (Cl^-, NO_3^-, SO_4^{2-}, CO_3^{2-}, PO_4^{3-}, Li^+, NH_4^+, Na^+, Cu^{2+}, Mg^{2+}, Ni^{2+}, Ca^{2+}, Fe^{3+}, and Al^{3+}) on Cr(VI) adsorption was investigated by maintaining the concentration of Cr(VI) and each of the coexisting ions at the same molar concentration of

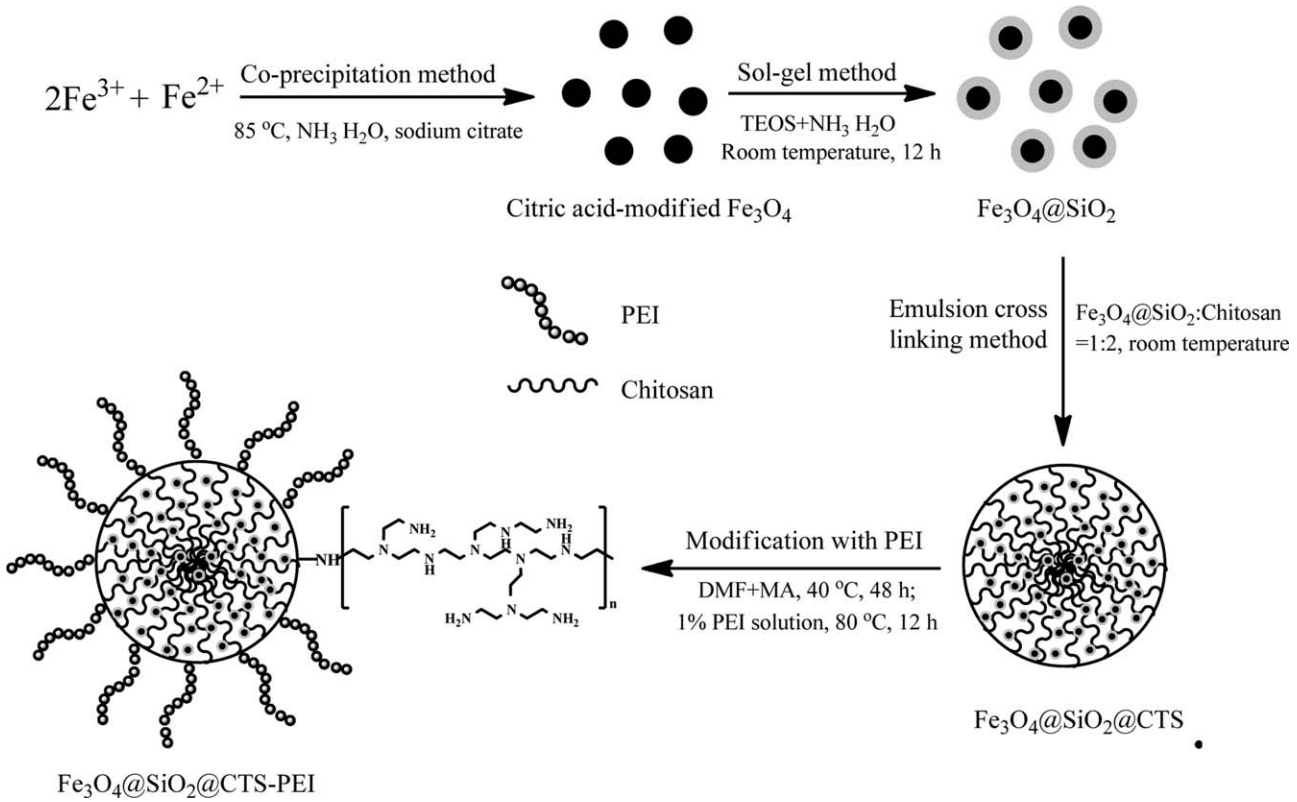

Scheme 1. Preparation of Fe_3O_4–SiO_2–CTS-PEI microspheres.

2.88 mmol/L [Cr(VI) mass concentration, 150 mg/L].[36] The 0.1 mol/L NaOH solution was used to regenerate the Cr(VI)-adsorbed adsorbent based on our previous works.[23,37] The Cr(VI) concentration was measured using an inductively coupled plasma atomic emission spectrometer (ICP-OES, Perkin Elmer Optima 7000DV, USA), and the adsorption capacity at time t (q_t, mg/g) was calculated by eq. (1):

$$q_t = \frac{(C_0 - C_t) \times V}{m} \quad (1)$$

where C_0 (mg/L) is the initial Cr(VI) concentration and C_t (mg/L) is the Cr(VI) concentration at time t (min), V (mL) is the volume of the medium, and m (mg) is the amount of adsorbent used.

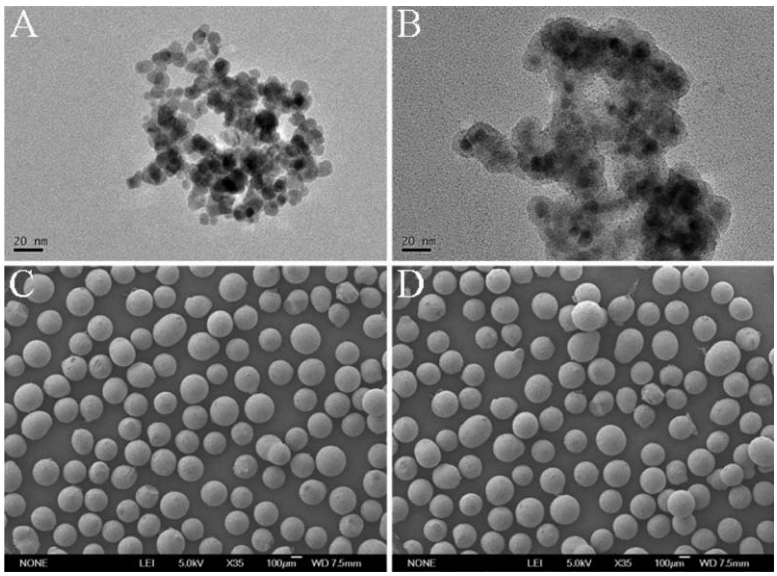

Figure 1. TEM or SEM images of (A) Fe_3O_4, (B) Fe_3O_4–SiO_2, (C) Fe_3O_4–SiO_2–CTS, and (D) Fe_3O_4–SiO_2–CTS-PEI.

Table I. Physical Properties of Fe_3O_4–SiO_2–CTS-PEI

Adsorbent	Particle size (μm)	Specific surface area (m^2/g)	Pore size (nm)	Porosity (%)	Fe_3O_4 (%)	SiO_2 (%)	Organic component (%)	Water (%)
Fe_3O_4-SiO_2-CTS-PEI	223.2	11.3	76.3	53.2	21.74	20.88	48.87	8.51

RESULTS AND DISCUSSION

Morphology and Specific Surface Area Analysis

Figure 1 shows the images of Fe_3O_4, Fe_3O_4–SiO_2, Fe_3O_4–SiO_2–CTS, and Fe_3O_4–SiO_2–CTS-PEI microspheres. The diameter of citric acid–modified Fe_3O_4 was 5–13 nm with a narrow size distribution. The Fe_3O_4–SiO_2 core–shell structure is found in Figure 1(B), indicating that the Fe_3O_4 nanoparticles were successfully coated with SiO_2, and the thickness of the silica shell was about 5 nm. It was interesting that one Fe_3O_4 nanoparticle to one SiO_2 coating layer was observed, which was attributed to the excellent dispersion of citric acid–modified Fe_3O_4 nanoparticles in the polar medium. The Fe_3O_4–SiO_2–CTS and Fe_3O_4–SiO_2–CTS-PEI microspheres had a spherical form with narrow size distribution (Figure 1C), and the average particle diameters of Fe_3O_4–SiO_2–CTS and Fe_3O_4–SiO_2–CTS-PEI were approximately 223.2 μm with no significant difference (Table I). According to the mercury porosimetry data, the average pore diameter and porosity of Fe_3O_4–SiO_2–CTS-PEI microspheres were evaluated to be 76.3 nm and 53.2%, respectively, indicating that the adsorbent had a macroporous structure. In addition, the microspheres had a relatively high specific surface area of 11.3 m^2/g according to the BET method.

FTIR and XRD Analysis

FTIR and XRD were used to characterize the synthesis route of Fe_3O_4–SiO_2–CTS-PEI. Figure 2A shows the FTIR spectra of Fe_3O_4, Fe_3O_4–SiO_2, Fe_3O_4–SiO_2–CTS, Fe_3O_4–SiO_2–CTS-MA, and Fe_3O_4–SiO_2–CTS-PEI. In the spectrum of Fe_3O_4, the peak at 582 cm^{-1} corresponds to the Fe—O vibration, the peak at 3414 cm^{-1} is assigned to the O—H vibration,[23] and the peaks at 2925 and 2858 cm^{-1} are characteristic of the C—H bond on the citric acid. In the Fe_3O_4–SiO_2 spectrum, the new peaks at 1090 and 800 cm^{-1} are attributed to the vibrations of the Si—O and Si—O—Fe bonds,[23] implying that SiO_2 was successfully grafted onto the Fe_3O_4 surface through chemical bonds. In the spectrum of Fe_3O_4–SiO_2–CTS, the absorbance peaks of the C—H bond greatly improved, and the new peak for the N—H bond in chitosan appeared at 1575 cm^{-1},[38] which indicated that the Fe_3O_4–SiO_2 nanoparticles were successfully coated with chitosan. In addition, the small peak at 1725 cm^{-1} showed the existence of the C═O bond in free aldehydic groups on the magnetic chitosan microspheres.[35] Compared with Fe_3O_4–SiO_2–CTS, in the Fe_3O_4–SiO_2–CTS-MA spectrum, the peak of the C═O bond at 1725 cm^{-1} increased to a large extent owing to the existence of ester groups on the MA. Finally, the peak at 1725 cm^{-1} disappeared in the spectrum of Fe_3O_4–SiO_2–CTS-PEI, suggesting that PEI was successfully reacted with the aldehydic and ester groups on the magnetic chitosan microspheres. The amino group capacities of Fe_3O_4–SiO_2–CTS and Fe_3O_4–SiO_2–CTS-PEI were determined as 2.3 ± 0.1 and 4.9 ± 0.3 mmol/g using the volumetric method. The higher amino group capacity on Fe_3O_4–SiO_2–CTS-PEI also confirmed that the magnetic chitosan microspheres were modified with PEI successfully. Figure 2B shows the XRD patterns of Fe_3O_4, chitosan Fe_3O_4–SiO_2–CTS, and Fe_3O_4–SiO_2–CTS-PEI. The six characteristic peaks appeared in Fe_3O_4 at 30.14°, 35.54°, 43.18°, 53.92°, 57.14°, and 62.80° and were assigned to the (220), (311), (400), (422), (511), and (440) planes of the pure Fe_3O_4 (JCPDS card No. 65-3107).[23] Chitosan itself showed typical peaks at 12.13° and 20.42°, which corresponded to a mixture of (101) and (002), and (001) and (100), respectively.[39] In the XRD patterns of Fe_3O_4–SiO_2–CTS and Fe_3O_4–SiO_2–CTS-PEI, the characteristic

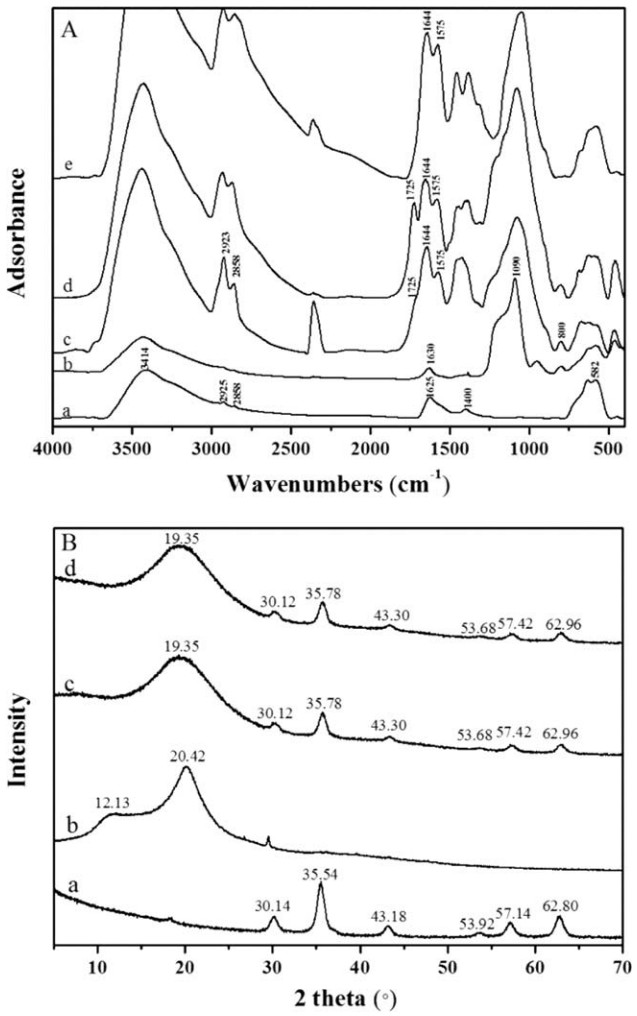

Figure 2. (A) FTIR spectra of (a) Fe_3O_4, (b) Fe_3O_4–SiO_2, (c) Fe_3O_4–SiO_2–CTS, (d) Fe_3O_4–SiO_2–CTS-MA and (e) Fe_3O_4–SiO_2–CTS-PEI, and (B) XRD patterns of (a) Fe_3O_4, (b) chitosan, (c) Fe_3O_4–SiO_2–CTS, and (d) Fe_3O_4–SiO_2–CTS-PEI.

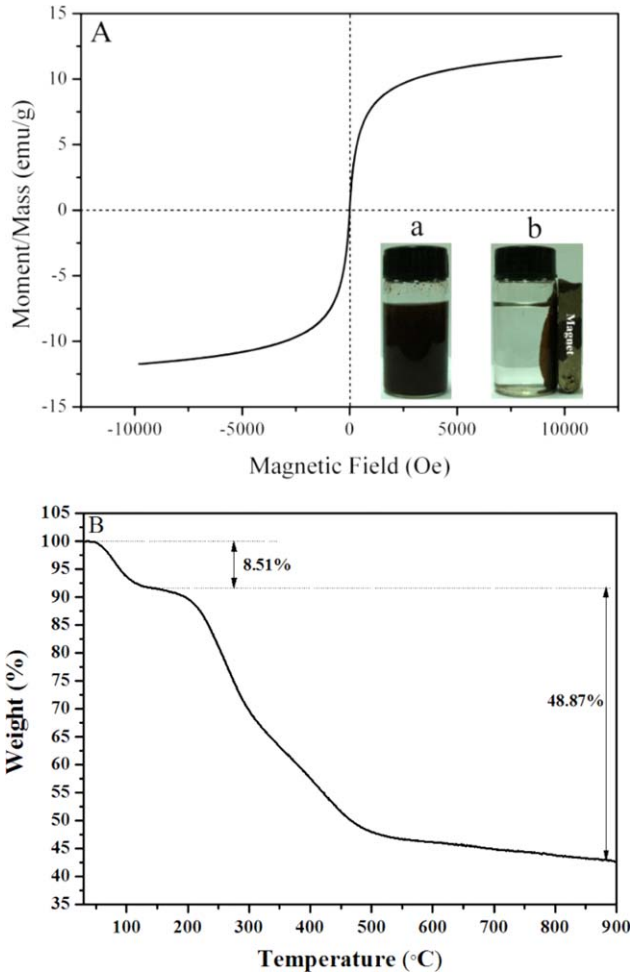

Figure 3. (A) Hysteresis loop and (B) TGA curves of the Fe_3O_4–SiO_2–CTS-PEI magnetic microspheres; the insert shows the magnetic separation of Fe_3O_4–SiO_2–CTS-PEI from aqueous solution by applying an external magnetic field, and the time from (a) to (b) was less than 30 s. [Color figure can be viewed in the online issue, which is available at wileyonlinelibrary.com.]

peaks of Fe_3O_4 and chitosan were observed, indicating that the magnetic silica nanoparticles were embedded in the chitosan matrix and the crystal structure of the Fe_3O_4 nanoparticles was unchanged.

Magnetic Property and TGA Analysis

The magnetic hysteresis loop and TGA curves of Fe_3O_4–SiO_2–CTS-PEI are shown in Figure 3. As shown in Figure 3A, the Fe_3O_4–SiO_2–CTS-PEI exhibited a typical superparamagnetic property due to the zero remanence and coercivity behaviors, and the saturated magnetization value (M_s) was 11.7 emu/g. With such high M_s, the microspheres showed a high magnetic responsiveness and could be quickly separated from the aqueous solution by a magnet. In the TGA curve of Fe_3O_4–SiO_2–CTS-PEI, weight loss occurred in two distinct stages. In the first stage, from 30°C to 150°C, there was a weight loss of about 8.51% related to the loss of adsorbed and bound water on the microspheres.[38] The second stage of weight loss (close to 48.87%), starting at around 150°C and completing by 900°C,

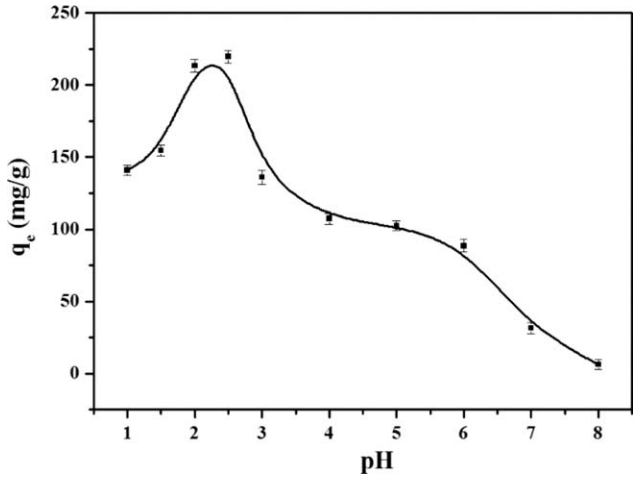

Figure 4. Effect of the pH on the adsorption of Cr(VI) onto Fe_3O_4–SiO_2–CTS-PEI microspheres (volume of the medium, 50 mL; initial Cr(VI) concentration, 150 mg/L; adsorbent dose, 0.025 g; contact time, 5 h; temperature, 25°C).

was attributed to the thermal decomposition of the surface chitosan layer. The Fe_3O_4–SiO_2 content in the microspheres could also be estimated as approximately 42.62% by the subtraction method. In addition, the Fe_3O_4 content of magnetic silica nanoparticles was analyzed by an ICP-OES analysis of the extract from the sample obtained with HCl (1:1) for 3 h at 90°C,[35] and it was determined as 51.0%. Therefore, the Fe_3O_4 content of Fe_3O_4–SiO_2–CTS-PEI was about 21.74% (Table I).

Solvent Resistance Analysis

In order to characterize the acid-resistant property of Fe_3O_4–SiO_2–CTS-PEI, the Fe_3O_4, Fe_3O_4–SiO_2, and Fe_3O_4–SiO_2–CTS-PEI were incubated in 15 mL of water at pH 2.0 at room temperature for 24 h. The Fe_3O_4 contents of Fe_3O_4, Fe_3O_4–SiO_2, and Fe_3O_4–SiO_2–CTS-PEI were maintained at 20 mg. The Fe_3O_4 nanoparticles were easily dissolved, and the color of the solution turned yellow immediately (Supporting Information,

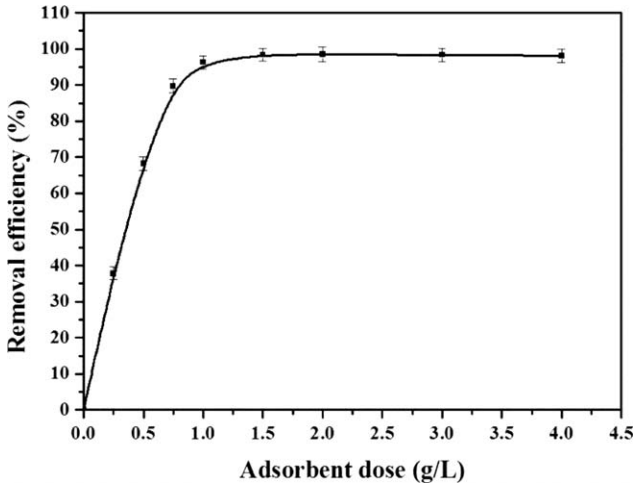

Figure 5. Effect of adsorbent dose on the removal efficiency of Cr(VI) by Fe_3O_4–SiO_2–CTS-PEI (pH, 2.5; volume of the medium, 50 mL; initial Cr(VI) concentration, 150 mg/L; contact time, 5 h; temperature, 25°C) .

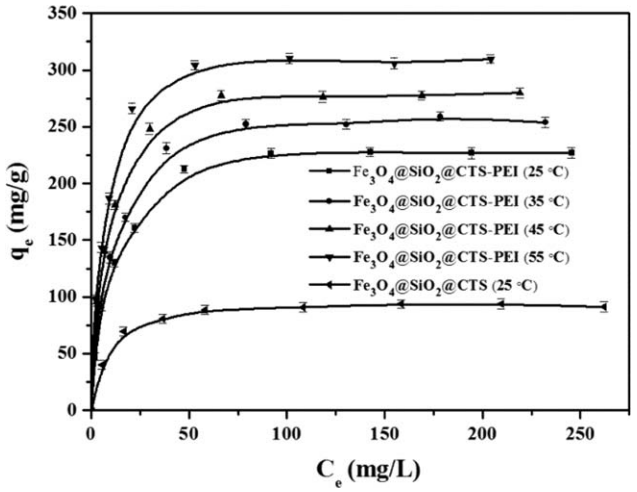

Figure 6. Adsorption isotherms of Cr(VI) onto Fe_3O_4–SiO_2–CTS-PEI microspheres at different temperatures of 25, 35, 45, and 55°C and Fe_3O_4–SiO_2–CTS at 25°C (pH, 2.5; volume of the medium, 50 mL; adsorbent dose, 0.025 g; contact time 2 h).

Figure S1). After 24 h, the color of the Fe_3O_4 suspension became deep yellow, while the Fe_3O_4–SiO_2 and Fe_3O_4–SiO_2–CTS-PEI suspensions were still colorless. The leaching Fe_3O_4 contents of Fe_3O_4, Fe_3O_4–SiO_2, and Fe_3O_4–SiO_2–CTS-PEI were analyzed by ICP-OES and measured as $6.64 \pm 0.39\%$, $0.27 \pm 0.03\%$, and $0.09 \pm 0.01\%$, respectively. These results indicated that the SiO_2 coating layer effectively improved the acid resistance of the inner magnetic cores. Also, no noticeable swelling was observed after 24 h, implying that the adsorbent had a strong swelling resistance.

Effect of pH and Adsorbent Dose on Cr(VI) Adsorption

The pH of the medium is one of the most important parameters, determining both the conversion of chromium species and the surface properties of the adsorbent. Aqueous Cr(VI) mainly exists in five forms: H_2CrO_4, $HCrO_4^-$, CrO_4^{2-}, $HCr_2O_7^-$, and $Cr_2O_7^{2-}$.[40] At pH above 6.0, CrO_4^{2-} is the main species, whereas $HCrO_4^-$ and $Cr_2O_7^{2-}$ are dominant at pH values of 2.0–6.0, and H_2CrO_4 is the major component at pH below 1.0. The effect of pH on the adsorption of Cr(VI) onto Fe_3O_4–SiO_2–CTS-PEI was carried out in the range of 1.0–8.0. As shown in Figure 4, it was clear that the adsorption capacity increased as the pH decreased from 8.0 to 2.5 and then decreased as the pH decreased from 2.5 to 1.0, and the maximum adsorption capacity was found at 2.5. The low adsorption capacity at pH above and below 2.5 should be attributed to the change of the Cr(VI) species and the amino group property on the adsorbent. Therefore, the optimized pH value of 2.5 was chosen to carry out the following experiments.

Figure 5 showed the effect of adsorbent dose on the removal efficiency of Cr(VI) from aqueous solution. It was clear that the removal efficiency increased quickly from 0 to 98.4% as the adsorbent dose increased from 0 to 1.5 g/L, and this was attributed to more active sites and surface area being available when the adsorbent dose improved. Following the critical dose of 1.5 g/L, the removal efficiency remained constant, indicating that the adsorption equilibrium was reached between the adsorbent and the Cr(VI) ions.

Adsorption Isotherm Study

The adsorption isotherm not only evaluates the adsorption capacity of the adsorbent, but also depicts the interaction pathway between adsorbate and adsorbent. Figure 6 showed the adsorption isotherms of Cr(VI) adsorption onto Fe_3O_4–SiO_2–CTS-PEI in the temperature range of 25–55°C and onto Fe_3O_4–SiO_2–CTS at 25°C. All of the curves for the adsorbents had a similar shape, which was very steep at the lower equilibrium concentrations and reached a maximum at an equilibrium Cr(VI) concentration of approximately 50 mg/L. It was obvious that the adsorption capacity of Fe_3O_4–SiO_2–CTS-PEI was significantly improved compared to that of Fe_3O_4–SiO_2–CTS, indicating that the improvement of the amino group content by PEI modification could obviously improve the adsorption capacity. In addition, it was found that the adsorption capacity increased with increasing temperature from 25°C to 55°C, which might be attributed to the increasing temperature benefiting the internal diffusion of Cr(VI) ions.

The Langmuir, Freundlich, and Temkin adsorption isotherm models were used to analyze the experimental data, which were expressed as follows[18]:

$$q_e = \frac{q_m K C_e}{1 + K C_e} \tag{2}$$

Table II. Adsorption Isotherm Parameters for the Adsorption of Cr(VI) onto Fe_3O_4–SiO_2–CTS-PEI and Fe_3O_4–SiO_2–CTS Microspheres at Different Temperatures

	Langmuir model			Freundlich model			Temkin model		
Temperature (°C)	q_m	K	R^2	K_f	n	R^2	a_T	b_T	R^2
25[a]	236.4	0.128	0.999	52.345	3.285	0.869	2.224	0.063	0.942
35[a]	265.3	0.138	0.999	58.038	3.205	0.884	2.446	0.058	0.949
45[a]	288.2	0.174	1.000	66.809	3.246	0.864	3.221	0.057	0.941
55[a]	317.5	0.211	1.000	75.846	3.217	0.866	3.969	0.054	0.937
25[b]	95.1	0.176	0.999	37.018	5.553	0.758	13.205	0.206	0.830

[a] Adsorption isotherm parameters for the adsorption of Cr(VI) onto Fe_3O_4–SiO_2–CTS-PEI.
[b] Adsorption isotherm parameters for the adsorption of Cr(VI) onto Fe_3O_4–SiO_2–CTS. Initial Cr(VI) concentration, 25 ~ 350 mg/L; pH, 2.5; and contact time, 2 h.

Table III. Adsorption Capacity Comparison of Various Magnetic Materials for the Removal of Cr(VI)

Adsorbents	Optimal pH	T (°C)	q_m (mg/g)	Refs.
Chitosan–iron(III) hydrogel	3.0	30	144.9	15
Chitosan-coated $MnFe_2O_4$	6.0	25	35.323	16
Chitosan/montmorillonite	2.0	30	35.71	17
EMCMCR	2.0	30	51.813	18
Magnetic chitosan beads	4.0	25	69.4	19
CAGS	2.0	25	58.48	39
CCGO	3.0	30	67.66	41
Chitosan nanoparticles	3.0	25	55.80	42
MCGO-IL	3.0	30	145.35	43
MCNCs	5.0	28	51.79	44
TEPA-NMPs	2.0	35	370.37	28
Poly(GMA-EGDMA)-PEI	2.0	25	140.6	30
Poly(MA-DVB)-EDA	3.0	20	231.8	34
Magnetic iron-nickel oxide	5.0	25	30	36
γ-Fe_2O_3–Fe_3O_4-PEI	2.2	25	78.13	45
Polypyrrole/Fe_3O_4	2.0	25	169.4	46
γ-Fe_2O_3–δ-FeOOH	2.5	25	25.8	47
Fe_3O_4–PAA-DETA	5.0	25	11.24	48
Biofunctional magnetic beads	1.0	28	5.79	49
Orange-like Fe_3O_4–PPy	2.0	25	209.2	50
γ-Fe_2O_3–chitosan	5.0	20	106.5	51
Fe_3O_4–PEIx-MMT	3.0	25	8.8	52
Fe–porous carbon	7.0	25	10.07	53
Ppy-Fe_3O_4/rGO	3.0	20	180.8	54
PPhSi-MNPs	3.0	25	35.21	55
MHCSs	3.0	25	200	56
MnO_2/Fe_3O_4/o-MWCNTs	2.0	22	170.4	57
nZVI–MG	3.0	30	101.0	58
Cyanex-301-coated SPION	2.0	23	30.8	59
PBGC-Fe/C	2.0	25	3.87	60
Fe/CMK-3	5.0	25	256.86	61
$ZnFe_2O_4$–Ce^{3+}	2.0	25	57.24	62
Magnetic gelatin	2.0	25	106.38	63
Fe_3O_4–SiO_2–CTS-PEI	2.5	25	236.4	This work

$$q_e = Kf C_e^{1/n} \quad (3)$$

$$q_e = \frac{RT}{b_T}\ln a_T + \frac{RT}{b_T}\ln C_e \quad (4)$$

where q_e (mg/g) and C_e (mg/L) are the adsorption capacity and Cr(VI) concentration at equilibrium, respectively. Here, q_m (mg/g) is the maximum adsorption capacity and K is the Langmuir constant related to adsorption energy; n and K_f [(mg/g)(L/mg)$^{1/n}$] are the Freundlich constants, which indicate the intensity and capacity of the adsorption, respectively; b_T (KJ/mol) and α_T (L/g) are the Temkin adsorption constants corresponding to the heat of sorption and the maximum binding energy, respectively. The adsorption isotherm parameters are summarized in Table II. The higher correlation coefficient (R^2) values of the Langmuir model demonstrated that the experimental data were fitted better with the Langmuir model than both the Freundlich model and the Temkin model, which indicated a monolayer coverage of the Cr(VI) ions onto the surface of adsorbent. Furthermore, the introduction of PEI obviously improved the adsorption capacity of Cr(VI) onto the adsorbent by approximately 2.5 times, and the adsorption capacities were proportional to the amino group capacities of the adsorbents. The q_m values of the Fe_3O_4–SiO_2–CTS-PEI and other magnetic materials are listed in Table III. It was clear that the

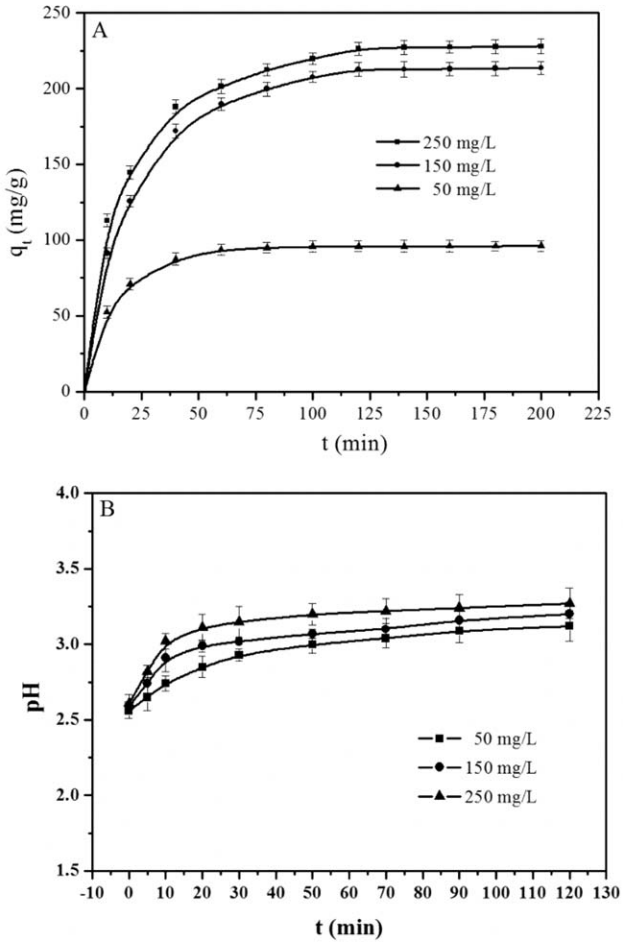

Figure 7. Effect of the contact time on adsorption and pH value at different initial Cr(VI) concentrations of 50, 150, and 250 mg/L (pH, 2.5; volume of the medium, 50 mL; adsorbent dose, 0.025 g; temperature, 25°C).

adsorption capacity of Fe_3O_4–SiO_2–CTS-PEI was much improved compared to those of other chitosan-based magnetic materials reported in the literature, and it also stayed at a high level compared to other types of magnetic adsorbents. In addition, in our previous works, magnetic poly(glycidyl methacrylate) microspheres, magnetic poly(vinyl alcohol) microspheres, and magnetic cellulose nanocomposite were developed and used as adsorbents for the removal of Cr(VI).[23,35,37] However, these adsorbents suffered from either weak acid resistance or low adsorption capacity. In contrast, the Fe_3O_4–SiO_2–CTS-PEI had the simultaneous advantages of strong acid resistance and high adsorption capacity, which should be a promising adsorbent in the application of Cr(VI) removal.

Adsorption Kinetic Study

Figure 7A shows the effect of contact time on the adsorption of Cr(VI) onto the Fe_3O_4–SiO_2–CTS-PEI at different initial concentrations ranging from 50 to 250 mg/L at 25°C. The kinetic curve for Cr(VI) ions shows that the adsorption was rapid at the beginning and reached equilibrium within 60–120 min. In addition, the change of pH value during adsorption was monitored. As shown in Figure 7B, the pH shows a trend similar to the adsorption capacity, which increased fast at the initial stage and reached equilibrium at around 30 min. This result demonstrated that the protonation time of amino groups was shorter than the adsorption time of Cr(VI), and the protonated amino groups could be used to adsorb the Cr(VI) by electrostatic interaction. The release of Fe_3O_4 to water during use was estimated as $0.05 \pm 0.01‰$, implying that the Fe_3O_4–SiO_2–CTS-PEI had a good acid resistance.

Three important kinetic models, i.e., a pseudo-first-order equation, a pseudo-second-order equation, and an intraparticle diffusion model, were used to simulate the kinetics of the adsorption process, which are expressed by eq. (5–7)[26]:

$$\log(q_e - q_t) = \log q_e - \left(\frac{K_1}{2.303}\right) t \tag{5}$$

$$\frac{t}{q_t} = \frac{1}{K_2 q_e^2} + \left(\frac{1}{q_e}\right) t \tag{6}$$

$$q_t = k_{id} t^{1/2} + c \tag{7}$$

where q_t and q_e (mg/g) are adsorption capacity at time t and equilibrium, respectively; K_1 (min^{-1}), K_2 [g/(mg min)], and K_{id} [mg/(g $min^{1/2}$)] are rate constants of the pseudo-first-order, pseudo-second-order, and intraparticle diffusion models, respectively; c (mg/g) is the intercept, corresponding to the thickness of the boundary layer. The plots of these adsorption kinetic models are shown in Figure S2 in the Supporting Information, and the obtained kinetic parameters are listed in Table IV. Because of the higher correlation coefficients and closer values between $q_{e,cal}$ and $q_{e,exp}$, the adsorption data were fitted better to the pseudo-second-order model than the pseudo-first-order model. This indicated that the adsorption rate of Cr(VI) onto Fe_3O_4–SiO_2–CTS-PEI might be controlled by chemical adsorption. For the intraparticle diffusion model, multilinearity and $K_{i,1} > K_{i,2} > K_{i,3}$ were observed, which could be described as follows. The first sharp portion corresponds to the external film diffusion stage, in which a large amount of Cr(VI) ions are adsorbed quickly onto the surface amino groups of adsorbent because the external film resistance was decreased by vigorous shaking. When the surface active sites are completely occupied, the Cr(VI) gradually enters the interior surface of pores in the second stage, in which intraparticle diffusion is the rate-controlling step. The intraparticle diffusion rate of the third portion is almost zero, suggesting that the final equilibrium stage is reached. In addition, none of the linear portions pass through the origin, implying that intraparticle diffusion is not the only rate-limiting step, and there might be two or more steps affecting the adsorption process.

Thermodynamic Study

To improve our understanding of the adsorption mechanism, the thermodynamic parameters, including Gibbs free energy change (ΔG^0), enthalpy change (ΔH^0), and entropy change (ΔS^0), were calculated using eq. (8 and 9)[64]:

$$\Delta G^0 = -RT \ln K_p \tag{8}$$

Table IV. Adsorption Kinetic Parameters for the Adsorption of Cr(VI) onto the Fe_3O_4–SiO_2–CTS-PEI Microspheres at Different Initial Concentrations

		Pseudo-first-order model			Pseudo-second-order model			Intraparticle diffusion model		
C_0 (mg/L)	$q_{e,exp}$ (mg/g)	K_1 (min^{-1})	$q_{e,cal}$ (mg/g)	R^2	K_2 [g/(mg min)]	$q_{e,cal}$ (mg/g)	R^2	$K_{i,1}$ [mg/(g $min^{1/2}$)]	$K_{i,2}$	$K_{i,3}$
50	96.1	0.035	33.0	0.927	0.0015	100.0	0.999	8.944	0.330	—
150	213.7	0.036	181.5	0.973	0.0003	232.0	0.999	25.443	8.734	0.329
250	228.0	0.036	184.6	0.975	0.0003	243.9	0.999	23.727	8.319	0.455

$$\ln K_p = -\frac{\Delta H^0}{RT} + \frac{\Delta S^0}{R} \quad (9)$$

where K_p is the thermodynamic equilibrium constant, i.e., the ratio of the equilibrium concentration of Cr(VI) on Fe_3O_4–SiO_2–CTS-PEI to that in solution, which is determined by plotting $\ln(q_e/C_e)$ versus q_e and extrapolating to zero q_e. The ΔH^0 and ΔS^0 could be calculated from the slope and intercept of the linear plot of $\ln K_p$ versus 1/T (Supporting Information, Figure S3) and were estimated as 4.67 KJ/mol and 0.027 KJ/(mol•K), respectively. The ΔG^0 at the temperatures of 298.15, 308.15, 318.15, and 328.15 K were calculated as −3.36, −3.61, −3.88 and −4.16 KJ/mol, respectively. The negative value of ΔG^0 and positive value of ΔH^0 indicated the spontaneous and endothermic nature of adsorption, while $\Delta S^0 > 0$ suggested the increase of randomness at the solid/solution interface during the adsorption process. The spontaneous and endothermic adsorption was reported for many adsorbents, such as PEI-grafted poly (GMA-EGDMA) microspheres,[30] EDA-modified magnetic poly (MA-DVB) microspheres,[34] and polypyrrole–Fe_3O_4 magnetic nanocomposite.[46]

Effect of Coexisting Ions and Reusability

The effect of the common coexisting ions (Cl^-, NO_3^-, SO_4^{2-}, CO_3^{2-}, PO_4^{3-}, Li^+, NH_4^+, Na^+, Cu^{2+}, Mg^{2+}, Ni^{2+}, Ca^{2+}, Fe^{3+}, and Al^{3+}) on Cr(VI) adsorption was investigated by maintaining the concentration of Cr(VI) and each of the coexisting ions at 2.88 mmol/L, and the initial pH value was kept at 2.5 (Figure 8). It was clear that the majority of these ions had no remarkable influence on the adsorption of Cr(VI) onto Fe_3O_4–SiO_2–CTS-PEI microspheres. Only SO_4^{2-} exhibited a slight competition for the active sites, owing to the high affinity between the SO_4^{2-} and amino groups.[35]

Furthermore, the reusability of the adsorbent was considered in the application of Cr(VI) removal. In this study, the Cr(VI)-loaded adsorbent was desorbed using a 0.1 mol/L NaOH solution and then washed with distilled water to the pH of 7.0 for reuse in the next run.[23,37] It was found that the desorption efficiency was approximately 92.5%, and the adsorption capacity was insignificantly charged after five adsorption–desorption cycles (Figure 9). These results indicated that the Fe_3O_4–SiO_2–CTS-PEI could be effectively regenerated and reused in the application of Cr(VI) removal from wastewater. Besides, the total leaching Fe_3O_4 content after five adsorption–desorption cycles was determined as 0.03 ± 0.01%, and the microsphere size was not remarkably changed, indicating that the adsorbent was stable during the repeated use cycles.

Adsorption Mechanisms

The adsorption process was always controlled by the surface properties of adsorbents, especially the functional groups on the adsorbent surface. The most widely reported mechanisms for adsorption included electrostatic attraction, ion exchange, hydrogen band, precipitation, complexation, and chelation.[65] In this work, it was obvious that the adsorption capacity was highly pH dependent. The amino groups (—NH_2, —NH—, and —N<) on the Fe_3O_4–SiO_2–CTS-PEI were easily protonated and positively charged (—NH_3^+, —NH_2^+—, and —NH^+<) under acidic conditions, which was confirmed in our previous works.[23,37] The electrostatic attraction happened between the adsorbent and chromium anions, which could be expressed as follows:

$$\begin{aligned} -NH_3^+/-NH_2^+-/-NH^+ &< +HCrO_4^- \rightarrow -NH_3^+/-NH_2^+-/-NH^+ \\ &< \cdots\cdots HCrO_4^- \end{aligned} \quad (10)$$

With the decrease of the pH value, the concentration of H^+ increased, and, hence, the protonation ability of amino groups

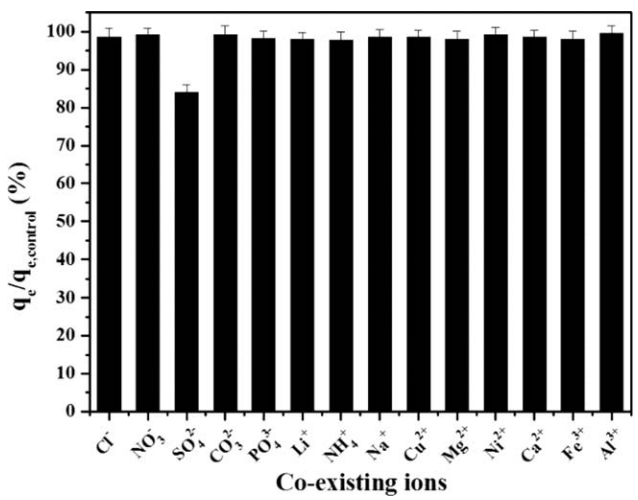

Figure 8. Effect of the common coexisting ions on the adsorption of Cr(VI) onto Fe_3O_4–SiO_2–CTS-PEI microspheres. The concentrations of Cr(VI) and each of the coexisting ions are maintained at 2.88 mmol/L, the initial pH value was kept at 2.5, and "control" signifies the lack of coexisting anions in conjunction with Cr(VI).

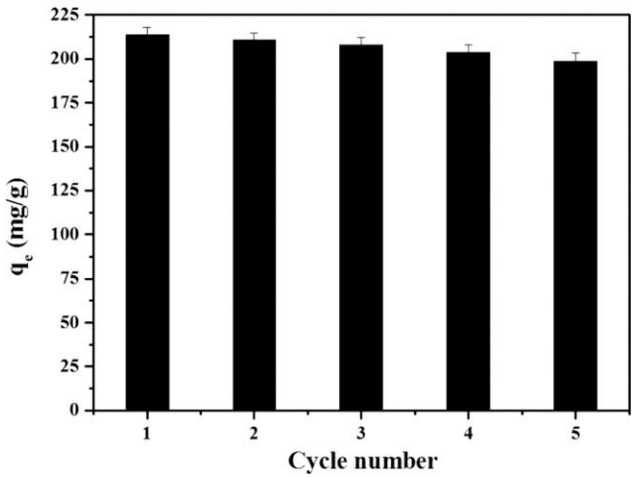

Figure 9. Performance of Fe_3O_4–SiO_2–CTS-PEI microspheres by five adsorption–desorption cycles of regeneration (adsorption conditions: pH, 2.5; volume, 50 mL; initial concentration, 150 mg/L; adsorbent dose, 0.025 g; contact time, 2 h; temperature, 25°C. Desorption conditions: eluent, 0.1 mol/L NaOH solution; volume, 5 mL; contact time, 2 h; temperature, 25°C).

was improved, which resulted in the increase of adsorption capacity at low pH value. The decrease of the adsorption capacity at the pH ranging from 2.5 to 1.0 was attributed to the formation of nonionic H_2CrO_4. Besides, the Cr(VI) anion was unstable in the presence of electron donors and exhibited a very high positive redox potential. Therefore, the reduction of Cr(VI) to Cr(III) might occur during the adsorption process, and the reduced Cr(III) ions could be subsequently complexed with the amino groups.[65,66] This assumption was proved by the Cr2p XPS spectrum. It was obvious that the adsorbed Cr state included Cr(VI) and Cr(III) (Figure 10). As discussed above, the Cr(VI) removal by Fe_3O_4–SiO_2–CTS-PEI should be governed by electrostatic adsorption coupled with reduction and complexation.

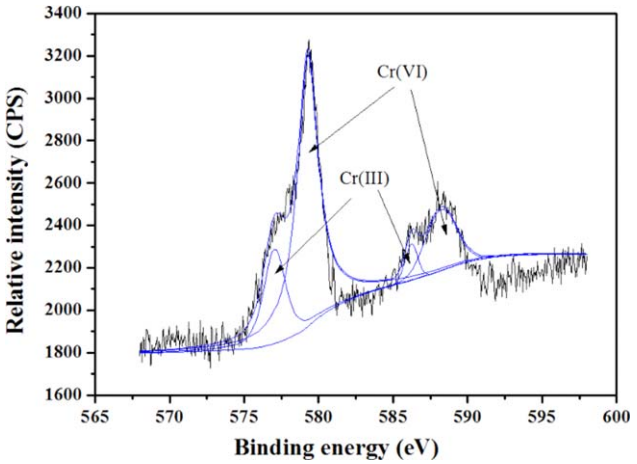

Figure 10. Cr2p XPS spectrum of the Cr-adsorbed Fe_3O_4–SiO_2–CTS-PEI microspheres. [Color figure can be viewed in the online issue, which is available at wileyonlinelibrary.com.]

CONCLUSIONS

In this study, a novel adsorbent for Cr(VI) removal, Fe_3O_4–SiO_2–CTS-PEI magnetic microspheres, was prepared under relatively mild conditions and characterized by TEM/SEM, FTIR, XRD, VSM, and TGA. The adsorbent exhibited high acid resistance and magnetic responsiveness. The leaching Fe_3O_4 content was only 0.09% after immersion in pH 2.0 water for 24 h, and the saturated magnetization of the adsorbent was 11.7 emu/g. Batch experiments demonstrated that the adsorbent had a high adsorption capacity, with the maximum adsorption capacity of 236.4 mg/g at 25°C. The adsorption process fit a pseudo-second-order model well and was spontaneous and endothermic in nature. The Fe_3O_4–SiO_2–CTS-PEI can be considered as an effective bioadsorbent for Cr(VI) removal from wastewater due to the advantages of high acid resistance, magnetic responsiveness, and adsorption capacity.

ACKNOWLEDGMENTS

This work was supported by the National Natural Science Foundation of China (No. 21106162), the National Key Natural Science Foundation of China (No. 21136009), and the Major Project of National Natural Science Foundation of China (No. 51090382).

REFERENCES

1. Kandasamy, P.; Sasidaran, M.; Kaliyappan, T. *J. Appl. Polym. Sci.* **2012**, *124*, 3600.
2. Wang, W. Q.; Li, M. Y.; Zeng, Q. X. *J. Appl. Polym. Sci.* **2012**, *126*, 1733.
3. Zhu, W. X.; Song, H.; Du, K. F.; Zeng, H.; Yao, S. *J. Appl. Polym. Sci.* **2013**, *128*, 2729.
4. Chowdhury, P.; Mondal, P.; Roy, K. *J. Appl. Polym. Sci.* **2011**, *119*, 823.
5. Sun, X.; Yang, L.; Xing, H.; Zhao, J.; Li, X.; Huang, Y.; Liu, H. *Colloids Surf. A* **2014**, *457*, 160.
6. Kong, Y.; Wei, J. X.; Wang, Z. L.; Sun, T.; Yao, C.; Chen, Z. D. *J. Appl. Polym. Sci.* **2011**, *122*, 2054.
7. Kara, A. *J. Appl. Polym. Sci.* **2009**, *114*, 948.
8. Gupta, V. K.; Ali, I.; Saleh, T. A.; Nayak, A.; Agarwal, S. *RSC Adv.* **2012**, *2*, 6380.
9. Gupta, V. K.; Srivastava, S. K.; Mohan, D.; Sharma, S. *Waste Manage.* **1997**, *17*, 517.
10. Bankar, A. V.; Kumar, A. R.; Zinjarde, S. S. *J. Hazard. Mater.* **2009**, *170*, 487.
11. Kumar, A. S. K.; Kalidhasan, S.; Rajesh, V.; Rajesh, N. *Ind. Eng. Chem. Res.* **2012**, *51*, 58.
12. Huang, R. H.; Yang, B. C.; Liu, Q. *J. Appl. Polym. Sci.* **2013**, *129*, 908.
13. Elwakeel, K. Z. *Desalination* **2010**, *250*, 105.
14. Sun, X. F.; Jing, Z. X.; Wang, H. H.; Li, Y. J. *J. Appl. Polym. Sci.* **2013**, *129*, 1555.
15. Yu, Z.; Zhang, X.; Huang, Y. *Ind. Eng. Chem. Res.* **2013**, *52*, 11956.

16. Xiao, Y.; Liang, H.; Chen, W.; Wang, Z. *Appl. Surf. Sci.* **2013**, *285P*, 498.
17. Chen, D.; Li, W.; Wu, Y.; Zhu, Q.; Lu, Z.; Du, G. *Chem. Eng. J.* **2013**, *221*, 8.
18. Hu, X. J.; Wang, J. S.; Liu, Y. G.; Li, X.; Zeng, G. M.; Bao, Z. L.; Zeng, X. X.; Chen, A. W.; Long, F. *J. Hazard. Mater.* **2011**, *185*, 306.
19. Huang, G.; Zhang, H.; Shi, J. X.; Langrish, T. A. G. *Ind. Eng. Chem. Res.* **2009**, *48*, 2646.
20. Burks, T.; Avila, M.; Akhtar, F.; Göthelid, M.; Lansåker, P. C.; Toprak, M. S.; Muhammed, M.; Uheida, A. *J. Colloid Interface Sci.* **2014**, *425*, 36.
21. Nethaji, S.; Sivasamy, A.; Mandal, A. B. *Bioresour. Technol.* **2013**, *134*, 94.
22. Wang, J.; Zhao, L.; Duan, W.; Han, L.; Chen, Y. *Ind. Eng. Chem. Res.* **2012**, *51*, 13655.
23. Sun, X.; Yang, L.; Li, Q.; Zhao, J.; Li, X.; Wang, X.; Liu, H. *Chem. Eng. J.* **2014**, *241*, 175.
24. Liu, Y. D.; Fang, F. F.; Choi, H. *J. Colloid Polym. Sci.* **2011**, *289*, 1295.
25. Wang, J.; Zheng, S.; Shao, Y.; Liu, J.; Xu, Z.; Zhu, D. *J. Colloid Interface Sci.* **2010**, *349*, 293.
26. Ren, Y.; Abbood, H. A.; He, F.; Peng, H.; Huang, K. *Chem. Eng. J.* **2013**, *226*, 300.
27. Denkbaş, E. B.; Kiliçay, E.; Birlikseven, C.; Öztürk, E. *React. Funct. Polym.* **2002**, *50*, 225.
28. Zhao, Y. G.; Shen, H. Y.; Pan, S. D.; Hu, M. Q.; Xia, Q. H. *J. Mater. Sci.* **2010**, *45*, 5291.
29. Gandhi, M. R.; Viswanathan, N.; Meenakshi, S. *Ind. Eng. Chem. Res.* **2012**, *51*, 5677.
30. Bayramoglu, G.; Yakuparica, M. *Chem. Eng. J.* **2008**, *139*, 20.
31. Ma, Y.; Liu, W. J.; Zhang, N.; Li, Y. S.; Jiang, H.; Sheng, G. P. *Bioresour. Technol.* **2014**, *169*, 403.
32. Xu, L.; Yang, L.; Luo, M.; Liang, X.; Wei, X.; Zhao, J.; Liu, H. *J. Hazard. Mater.* **2011**, *189*, 787.
33. Yuan, Q.; Li, N.; Chi, Y.; Geng, W.; Yan, W.; Zhao, Y.; Li, X.; Dong, B. *J. Hazard. Mater.* **2013**, *254–255*, 157.
34. Wang, Q.; Guan, Y.; Liu, X.; Ren, X.; Yang, M. *J. Colloid Interface Sci.* **2012**, *375*, 160.
35. Sun, X.; Yang, L.; Xing, H.; Zhao, J.; Li, X.; Huang, Y.; Liu, H. *Chem. Eng. J.* **2013**, *234*, 338.
36. Wei, L.; Yang, G.; Wang, R.; Ma, W. *J. Hazard. Mater.* **2009**, *164*, 1159.
37. Sun, X.; Yang, L.; Li, Q.; Liu, Z.; Dong, T.; Liu, H. *Chem. Eng. J.* **2015**, *262*, 101.
38. Zhu, H. Y.; Jiang, R.; Xiao, L.; Zeng, G. M. *Bioresour. Technol.* **2010**, *101*, 5063.
39. Abou El-Reash, Y. G.; Otto, M.; Kenawy, I. M.; Ouf, A. M. *Int. J. Biol. Macromol.* **2011**, *49*, 513.
40. Saha, B.; Orvig, C. *Coord. Chem. Rev.* **2010**, *254*, 2959.
41. Li, L.; Fan, L.; Sun, M.; Qiu, H.; Li, X.; Duan, H.; Luo, C. *Colloids Surf. B* **2013**, *107*, 76.
42. Thinh, N. N.; Hanh, P. T. B.; Ha, L. T. T.; Anh, L. N.; Hoang, T. V.; Hoang, V. D.; Dang, L. H.; Khoi, N. V.; Lam, T. D. *Mater. Sci. Eng. C* **2013**, *33*, 1214.
43. Li, L.; Luo, C.; Li, X.; Duan, H.; Wang, X. *Int. J. Biol. Macromol.* **2014**, *66*, 172.
44. Xiao, Y.; Liang, H.; Wang, Z. *Mater. Res. Bull.* **2013**, *48*, 3910.
45. Pang, Y.; Zeng, G.; Tang, L.; Zhang, Y.; Liu, Y.; Lei, X.; Li, Z.; Zhang, J.; Liu, Z.; Xiong, Y. *Chem. Eng. J.* **2011**, *175*, 222.
46. Bhaumik, M.; Maity, A.; Srinivasu, V. V.; Onyango, M. S. *J. Hazard. Mater.* **2011**, *190*, 381.
47. Hu, J.; Lo, I. M. C.; Chen, G. *Sep. Purif. Technol.* **2007**, *58*, 76.
48. Huang, S. H.; Chen, D. H. *J. Hazard. Mater.* **2009**, *163*, 174.
49. Li, H.; Li, Z.; Liu, T.; Xiao, X.; Peng, Z.; Deng, L. *Bioresour. Technol.* **2008**, *99*, 6271.
50. Wang, Y.; Zou, B.; Gao, T.; Wu, X.; Lou, S.; Zhou, S. *J. Mater. Chem.* **2012**, *22*, 9034.
51. Jiang, Y. J.; Yu, X. Y.; Luo, T.; Jia, Y.; Liu, J. H.; Huang, X. J. *J. Chem. Eng. Data* **2013**, *58*, 3142.
52. Larraza, I.; López-Gónzalez, M.; Corrales, T.; Marcelo, G. *J. Colloid Interface Sci.* **2012**, *385*, 24.
53. Zhuang, L.; Li, Q.; Chen, J.; Ma, B.; Chen, S. *Chem. Eng. J.* **2014**, *253*, 24.
54. Wang, H.; Yuan, X.; Wu, Y.; Chen, X.; Leng, L.; Wang, H.; Li, H.; Zeng, G. *Chem. Eng. J.* **2015**, *262*, 597.
55. Badruddoza, A. Z. M.; Shawon, Z. B. Z.; Rahman, M. T.; Hao, K. W.; Hidajat, K.; Uddin, M. S. *Chem. Eng. J.* **2013**, *225*, 607.
56. Zhang, L. H.; Sun, Q.; Liu, D. H.; Lu, A. H. *J. Mater. Chem. A* **2013**, *1*, 9477.
57. Luo, C.; Tian, Z.; Yang, B.; Zhang, L.; Yan, S. *Chem. Eng. J.* **2013**, *234*, 256.
58. Lv, X.; Xue, X.; Jiang, G.; Wu, D.; Sheng, T.; Zhou, H.; Xu, X. *J. Colloid Interface Sci.* **2014**, *417*, 51.
59. Burks, T.; Uheida, A.; Saleemi, M.; Eita, M.; Toprak, M. S.; Muhammed, M. *Sep. Sci. Technol.* **2013**, *48*, 1243.
60. Zhu, Z.; Zhu, Y.; Yang, F.; Zhang, X.; Qin, H.; Liang, Y.; Liu, J. *Desalin. Water Treat.* **2014**, *52*, 3133.
61. Tang, L.; Yang, G. D.; Zeng, G. M.; Cai, Y.; Li, S. S.; Zhou, Y. Y.; Pang, Y.; Liu, Y. Y.; Zhang, Y.; Luna, B. *Chem. Eng. J.* **2014**, *239*, 114.
62. Kuai, S.; Zhang, Z.; Nan, Z. *J. Hazard. Mater.* **2013**, *250–251*, 229.
63. Chen, G.; Qiao, C.; Wang, Y.; Yao, J. *Ind. Eng. Chem. Res.* **2014**, *53*, 15576.
64. Badruddoza, A. Z. M.; Tay, A. S. H.; Tan, P. Y.; Hidajat, K.; Uddin, M. S. *J. Hazard. Mater.* **2011**, *185*, 1177.
65. Deng, S.; Ting, Y. P. *Environ. Sci. Technol.* **2005**, *39*, 8490.
66. Shen, H.; Chen, J.; Dai, H.; Wang, L.; Hu, M. *Ind. Eng. Chem. Res.* **2013**, *52*, 12723.